Effects of vibrational entropy on the Al–Si phase diagram

2005 J. Phys.: Condens. Matter 17 2197

(http://iopscience.iop.org/0953-8984/17/13/017)

INSTITUTE OF PHYSICS PUBLISHING JOURNAL OF PHYSICS: CONDENSED MATTER

J. Phys.: Condens. Matter **17** (2005) 2197–2210 doi:10.1088/0953-8984/17/13/017

Effects of vibrational entropy on the Al–Si phase diagram

V Ozoliņš[1,4], B Sadigh[2] and M Asta[3]

[1] Department of Materials Science and Engineering, University of California, Los Angeles, CA 90095-1595, USA
[2] Lawrence Livermore National Laboratories, Livermore, CA 94551, USA
[3] Department of Materials Science and Engineering, Northwestern University, Evanston, IL 60208-3108, USA

E-mail: vidvuds@ucla.edu

Received 12 November 2004, in final form 12 November 2004
Published 18 March 2005
Online at stacks.iop.org/JPhysCM/17/2197

Abstract

An Al–Si solid-state phase diagram is studied using first-principles electronic structure calculations of formation enthalpies and quasiharmonic vibrational free energies. The harmonic vibrational entropy of formation of a Si impurity in fcc Al is predicted to be $\Delta S_{\mathrm{vib}} = +2.6\, k_{\mathrm{B}}$ per Si atom, resulting in more than a ten-fold increase in the calculated solubility. Thermal expansion is found to further increase the maximum solubility at $T = 850$ K by approximately 55%. Surprisingly, when vibrational effects are included, the widely used local-density approximation (LDA) performs poorly in reproducing the experimental solvus boundary, which is overestimated by a factor of ten. This failure is attributed to the neglect of corrections to the calculated LDA impurity enthalpy ΔH stemming from the inhomogeneity of the electronic charge density. These corrections tend to favour the four-fold coordinated diamond structure over the twelve-fold coordinated fcc solid-solution phase. The generalized-gradient approximation (GGA) is found to remove most of the discrepancy between the experimental and calculated ΔH, giving a good agreement with the experimental Al–Si phase diagram.

1. Introduction

Ab initio prediction of alloy composition–temperature (c–T) phase diagrams remains a central goal for the development of first-principles methods in computational materials science research. During recent years, many studies have demonstrated remarkable success in *ab initio* calculations of c–T phase diagrams for a wide variety of metals, semiconductors and ionic materials [1–5]. These studies are based upon a convenient parametrization of

[4] Author to whom any correspondence should be addressed.

the configurational energy in terms of a generalized Ising model with pair and multibody interactions [6]. Generally, first-principles calculated phase diagrams exhibit the correct topology and sometimes even predict new, unsuspected ordered phases. Unfortunately, the quantitative accuracy of *ab initio* calculated phase boundaries is usually well below the requirements of most practical applications [7]. Recently, the accuracy of *ab initio* calculated alloy free energies has been improved through the incorporation of non-configurational contributions to excess entropies arising from, for example, electronic and vibrational excitations [8–16]. This work has been motivated by recent measurements of large excess entropies due to ionic vibrations [17–23], even when the structures of competing phases are based upon a common underlying lattice framework.

The present study deals with the absolute accuracy that can be achieved in state-of-the-art first-principles calculations of phase diagrams by including quasiharmonic vibrational contributions to the free energies. We consider the technologically relevant Al–Si alloy system, which has a well-studied c–T phase diagram [24] of the simple eutectic type with two terminal solid-solution phases: fcc-based (Al) and diamond-structure (Si). The (Al) solid-solution phase extends to roughly 1.6 at.% Si at $T = 850$ K [25, 26], while lattice parameter measurements indicate that the solubility of Al in Si is negligibly small [27, 28]. The (Al) and (Si) phase-fields are separated by a large two-phase region; intermediate compounds do not exist. Due to the dilute nature of both solid-solution phases, the temperature-dependent solubility limit $c_s(T)$ of Si in fcc Al is given accurately by the following formula:

$$c_s(T) = \exp\left[\frac{-\Delta G}{k_B T}\right], \tag{1}$$

where ΔG is the excess free energy for a dilute Si atom in fcc Al, expressed per Si atom as:

$$\Delta G = \Delta H - T\Delta S_{nc}. \tag{2}$$

ΔH is the enthalpy of formation per Si atom and ΔS_{nc} is the non-configurational entropy, including vibrational and electronic contributions, but excluding the ideal entropy of mixing, $S_{conf} = -k_B[c \ln c + (1 - c)\ln(1 - c)]$. Reference states for the formation quantities in equation (2) are pure diamond Si and fcc Al. Using equation (2) one obtains that the solvus boundary is given by:

$$c_s(T) = e^{\Delta S_{nc}/k_B} e^{-\Delta H/k_B T}. \tag{3}$$

If the temperature-dependence of ΔS_{nc} and ΔH is small, as in the case of weakly anharmonic crystals [29], the non-configurational entropy contributes a constant prefactor, $e^{\Delta S_{nc}/k_B}$, multiplying the ideal solubility, $c_0(T) = e^{-\Delta H_0/k_B T}$, where ΔH_0 is the excess enthalpy at $T = 0$ K. Equations (1)–(3) are valid whenever the interaction between impurities is statistically negligible, a condition which is well satisfied for compositions below 1–2 at.%, i.e. in the range relevant for the Al–Si phase diagram. Simplicity of the configurational thermodynamics represented by equations (1)–(3) allows us to separate the effects of impurity energetics from the effects of ionic vibrations on the phase boundaries in the Al–Si system.

We find that in spite of its apparent simplicity, the Al–Si system presents a challenging test case for first-principles methods. Theoretical calculations based upon the density functional theory (DFT) [30] reveal a large vibrational contribution to the Gibbs free energy of a Si impurity. The non-configurational entropy, ΔS_{nc}, is found to be approximately 2.6 k_B per impurity atom. According to equation (3), this contribution significantly enhances the calculated solubility limit on the Al-rich side of the phase diagram. Softening of the lattice phonons around the Si impurity is found to be responsible for such a large effect. An analysis of the experimental solubility data confirms this trend, revealing a significant entropy prefactor

in equation (3). Unexpectedly, when the local-density approximation (LDA) to the electronic exchange–correlation functional is used to obtain the formation enthalpies ΔH, the vibrational entropy contribution is found to degrade the agreement between the experimentally determined and theoretically calculated solvus boundaries. This failure is attributed to the inability of the LDA to correctly capture total energy differences between competing phases. In particular, the binding energy of a Si atom in the four-fold coordinated diamond structure is underestimated relative to the binding energy of a Si impurity in the twelve-fold coordinated solid-solution fcc phase. We suggest that the correct formation energy ΔH can be obtained only by taking into account corrections to the LDA arising from charge inhomogeneity. For instance, we demonstrate that the generalized gradient approximation of Perdew and Wang [31] increases the calculated formation energy of a Si impurity by approximately +0.15 eV, removing the bulk of the discrepancy between the calculated and measured solubilities. This improvement can be attributed to the tendency of the GGA to favour the more inhomogeneous charge distribution in the diamond structure relative to the metallic fcc-based solid solution phase. These findings show that Al–Si represents an interesting example where both the vibrational free energies and gradient corrections are needed to calculate an accurate phase diagram.

2. Methods

The free energy ΔG in equation (1) was calculated using first-principles density functional theory [30]. The results were sensitive to the chosen exchange–correlation energy functional; we present a comparison of the popular local-density approximation (LDA) parameterized by Perdew and Zunger [32], with the generalized gradient approximation (GGA) developed by Perdew and Wang [31]. The numerical accuracy of the calculated excess free energies was verified using two different pseudopotential-based techniques. The first method was based on standard norm-conserving pseudopotentials (NCPP), generated using the prescription of Troullier and Martins [33]. Pseudopotentials were generated for valence electron configurations $3s^2 3p^{0.99} 3d^{0.01}$ for Al and $3s^2 3p^{1.9} 3d^{0.1}$ for Si. Another set of calculations was performed using the ultrasoft pseudopotential technique [34] and the Vienna *Ab initio* Simulation Package (VASP), developed at the Institut für Material-physik of the Universität Wien [35–38]. Both methods include corrections due to the non-linearity of the core–valence exchange–correlation functional [39]. The electronic wavefunctions were expanded in plane wave bases with cutoff energies $E_{\mathrm{cut}} = 326.5$ and 100 eV for norm-conserving and ultrasoft pseudopotentials, respectively. Electronic states were sampled on equivalent $\mathbf{k}$ point grids containing 16 384 points in the full Brillouin zone of the fcc lattice and populated according to a finite-temperature ($T = 27$ meV) Fermi–Dirac broadening scheme.

LDA phonon spectra were obtained using an implementation of the first-principles linear response (LR) theory [40, 41] using the plane wave basis set and NCPP [42]. The linear response method allows the calculation of the properties of phonons of a given wavelength without resorting to expensive finite-difference frozen phonon calculations on large supercells. Numerical convergence of the impurity free energies was ensured by using equivalent [43] reciprocal space grids for both phonon and electron states. Dynamical matrices and phonon states were calculated on regular grids of phonon wavevectors $\mathbf{q}$ (we used regular $3 \times 3 \times 3$ and $2 \times 2 \times 2$ meshes for 27-atom and 32-atom supercells, respectively). For diamond Si electron and phonon states were both sampled on a $8 \times 8 \times 8$ regular grid. Interatomic force constants were extracted by applying the inverse Fourier transform to the directly calculated dynamical matrices. Phonon mode Grüneisen parameters, $\gamma_{\mathbf{q}n} = -\frac{\mathrm{d} \ln \omega_{\mathbf{q}n}}{\mathrm{d} \ln V}$, were obtained from finite differences by calculating phonon frequencies at two volumes separated by $\approx 3\%$.

Since our linear response code cannot handle gradient corrections, GGA phonon calculations for Si impurities in Al were performed using the VASP code and the frozen phonon method [44]. We studied $\mathbf{k} = 0$ phonon states of 32-atom and 64-atom cubic impurity supercells. To ensure maximum cancellation of numerical errors, the excess free energies of Si impurities were obtained by subtracting the vibrational entropies of fcc Al calculated using exactly the same cells and numerical parameters. For each cell, all symmetry inequivalent rows of the $\mathbf{q} = 0$ dynamical matrix were determined (there are 8 and 13 such rows for the 32-atom and 64-atom cells, respectively); the remaining rows were obtained using standard symmetry-group transformations [45]. Individual elements $D^{ij}_{\alpha\beta}$ of the $\mathbf{q} = 0$ dynamical matrix are proportional to the force acting on the atom i along the Cartesian direction α if the atom j is displaced by a small amount along the direction β, $F^i_\alpha = -\sqrt{M_i M_j} D^{ij}_{\alpha\beta} u^j_\beta$. For each symmetry-inequivalent choice of u^j_β, the forces F^i_α were obtained for a set of 11 evenly distributed displacements around the equilibrium position, from $u^j_\beta = -0.05$ Å to $u^j_\beta = +0.05$ Å. The calculated Hellman–Feynman forces were fitted using third-order splines, and the linear terms were used to extract $D^{ij}_{\alpha\beta}$. The numerical accuracy of this method was established by comparing the LDA phonon spectra of Si impurities with the results obtained using the linear response method. The calculated phonon frequencies agreed to within a few per cent (see section 3.1).

3. Results

3.1. LDA impurity free energies

We have calculated structural, elastic and vibrational properties of fcc Al, diamond Si and several fcc-based impurity supercells: a cubic 32-atom cell ($Al_{31}Si$), a 27-atom $3 \times 3 \times 3$ cell ($Al_{26}Si$), and a 64-atom $4 \times 4 \times 4$ cell ($Al_{63}Si$). The results obtained using the LDA are given in the upper part of table 1. The calculated $T = 0$ K formation enthalpies of a Si impurity in fcc Al are $\Delta H_0 = +0.309$ eV using norm-conserving pseudopotentials and $\Delta H_0 = +0.314$ eV using VASP and ultrasoft pseudopotentials. These numbers are in reasonable agreement with the earlier values of $\Delta H_0 = +0.37$ and +0.38 eV obtained by Chetty *et al* [48] and Turner *et al* [49], respectively. Slight differences in the calculated ΔH_0 are probably caused by numerical factors (plane wave energy cutoffs, number of $\mathbf{k}$ points, or supercell size), use of different pseudopotentials (nonlinear core correction, pseudopotential core radii), or both. We have checked that further increases of the cell size or of the number of $\mathbf{k}$ points lead to negligible changes in the calculated ΔH_0, therefore the values given in table 1 are numerically converged for the present choice of pseudopotentials.

Neglecting all other free energy contributions, an impurity formation energy of $\Delta H_0 = +0.31$ eV results in a calculated solubility of 1.4 at.% at $T = 850$ K, which is very close to the experimental value of 1.6 at.% [50]. Such a close agreement seems to indicate that the LDA performs very well in describing the solvus boundary in Al–Si. However, we will argue that this result is fortuitous and that a proper treatment of vibrational effects destroys the apparent accord between the LDA and the experimental solubility data. Indeed, as seen from table 1, the vibrational entropy of a Si impurity is calculated to be $\Delta S_{\mathrm{vib}} = +1.8\, k_{\mathrm{B}}$ per Si atom using the 32-atom cell and $\Delta S_{\mathrm{vib}} = +2.3\, k_{\mathrm{B}}$ per Si atom using the 64-atom cell. With these values of ΔS_{nc}, equation (3) predicts a six- to ten-fold increase in the calculated LDA solubility. We conclude that *accounting for vibrational entropy contributions in equation* (1) *reveals that the LDA severely overestimates the solubility of Si in Al.*

To ascertain that the above discrepancy is not caused by an error in the calculated vibrational entropy of a Si impurity, we have performed an independent calculation of ΔS_{vib}

Table 1. Calculated equilibrium atomic volumes V_0, bulk moduli B_0, average Grüneisen parameters γ_G, excess enthalpies ΔH, excess harmonic vibrational entropies ΔS_{vib}, and high-temperature coefficients of volume thermal expansion $\beta = \frac{1}{V}\left(\frac{\partial V}{\partial T}\right)_p$. The last column gives the rate of increase in the excess vibrational entropy due to thermal expansion, $\frac{d}{dT}\Delta S_{vib}$. All excess quantities are given per Si impurity. Numbers in parentheses represent experimental thermal expansion data [46, 47].

Composition	V_0 (Å^3)	B_0 (GPa)	B'	γ_G	β (10^6 K^{-1})	ΔV_0 (Å^3)	ΔH (meV)	ΔS_{vib} (k_B)	$\frac{d}{dT}\Delta S_{vib}$ (10^{-3} k_B K^{-1})
LDA-NCPP linear response results									
Al	15.63	83	4.3	2.03	66(69)				
$Al_{26}Si$	15.52	85	4.6			−6.6	+347	+2.2	
$Al_{31}Si$	15.55	85	4.5	2.09	65	−6.5	+313	+1.8	0.88
$Al_{63}Si$	15.59					−6.2	+309		
Si	19.53	96	4.2	0.55	12(12)				
LDA-VASP frozen phonon results									
Al	15.78	82	4.4						
$Al_{31}Si$	15.70	83	4.8			−6.4	+327	+1.9	
$Al_{63}Si$	15.74	83	4.3			−6.2	+314	+2.3	
Si	19.60	95	4.1						
GGA-VASP frozen phonon results									
Al	16.55	73	4.4						
$Al_{31}Si$	16.48	73	4.5			−6.3	+468	+2.4	
$Al_{63}Si$	16.51	74	4.5			−6.3	+463	+2.6	
Si	20.34	87	4.2						

using the VASP code [35–38] and ultrasoft pseudopotentials [34] included in its standard distribution. We calculated all $\mathbf{q} = 0$ phonons in the 32-atom and 64-atom impurity cells using the frozen phonon technique. For the 32-atom cell, we obtained an excess vibrational entropy $\Delta S_{vib} = +1.9\ k_B$ per Si atom (see table 1), which should be compared with $+1.5\ k_B$ found from the linear response calculation using only the zone-centre phonons in the 32-atom impurity cell (the value $\Delta S_{vib} = +1.8\ k_B$ quoted in table 1 is for a $2 \times 2 \times 2$ mesh of phonon wavevectors). Direct inspection showed that the calculated phonon frequencies differed by only a few per cent. Considering the numerical uncertainties involved in taking a difference of two large numbers to obtain a small formation entropy, this is a very good level of agreement between two independent electronic-structure techniques. From the difference in vibrational entropies between the 32-atom and 64-atom supercells (see table 1), we estimate that the calculated vibrational entropy of the Si impurity is converged to better than $0.4\ k_B$. The uncertainty in ΔS_{vib} due to cell size effects will affect the solubility $c_s(T)$ by a relatively small amount (<50%). Finally, we also checked that increasing the total number of electronic **k** points in the full Brillouin zone from 16 384 to 55 296 had a negligible effect on the calculated phonon frequencies.

Additional evidence pointing to the importance of non-configurational effects is revealed by an analysis of the experimental data on Si solubility using equation (3). The most accurate and consistent data set for a range of temperatures has been provided by Dix and Heath [25], who used long annealing times and micrographic analyses to look for Si precipitates. It is thought that their data represent thermodynamic equilibrium down to approximately 350 °C [51]. Their results are shown as filled symbols in figure 1. Based upon equation (1), we have analysed

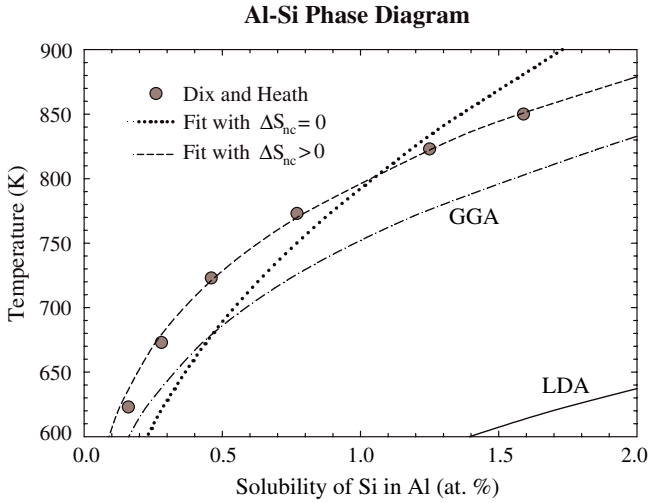

Figure 1. Solvus boundary in the binary Al–Si system. Experimental data of Dix and Heath [25] are shown as symbols. The solid line represents the first-principles calculated result using equation (3) and the LDA values of enthalpy ($\Delta H = +0.31$ eV) and vibrational entropy ($\Delta S_{\rm nc} = +2.3\ k_{\rm B}$). The GGA result ($\Delta H = +0.46$ eV and $\Delta S_{\rm nc} = +2.6\ k_{\rm B}$) is shown as a dash–dotted line. Also shown are fits of the experimental solubility data assuming $\Delta S_{\rm nc} = 0$ (dotted line) and $\Delta S_{\rm nc} \neq 0$ (dashed line) in equation (3) (see section 3.1). Effects of thermal expansion have not been included in these curves.

these data in two different ways. First, assuming that $\Delta S_{\rm nc} = 0$, ΔH can be estimated from a best fit to the experimental data points. This recipe yields $\Delta H = +315$ meV/atom, and predicts a solvus boundary that is in rather poor agreement with the experimental data at lower temperatures, as shown by the dotted line in figure 1. In the second step, we vary both $\Delta S_{\rm nc}$ and ΔH, which produces values $\Delta S_{\rm nc} = +2.7\ k_{\rm B}$ and $\Delta H = +504$ meV per Si atom. The resulting fit is shown as a dashed line in figure 1, reproducing the experimental data points extremely well. Incidentally, the latter enthalpy agrees with the value $\Delta H = +510$ meV quoted by Hatch [50], but is much larger than any of the LDA results quoted above. Furthermore, the extracted non-configurational entropy is consistent with the results of our linear response calculations, which find a large vibrational excess entropy. This analysis supports the conclusion that vibrational effects lead to a significant enhancement of the Si solid solubility.

So far we have demonstrated that the LDA severely underestimates the impurity formation enthalpy ΔH and overestimates the solubility of Si in Al by a factor of ten. Inclusion of the vibrational entropy term is crucial for uncovering this failure of the LDA, since in the absence of the exponential pre-factor $\exp[\Delta S_{\rm vib}/k_{\rm B}]$ in equation (3), the predicted LDA solubility at high temperatures would be in a very good agreement with the experimental data.

3.2. Harmonic phonons in Al–Si

Here we analyse physical effects contributing to the large excess vibrational entropy of a Si impurity. Figure 2 shows the calculated phonon densities of states (DOS) of fcc Al, diamond Si and a 32-atom Si impurity supercell. The latter DOS has been decomposed into contributions from the Si impurity and from the surrounding near-neighbour shells of Al atoms:

$$g_i(\omega) = \frac{1}{M} \sum_{\mathbf{q}} \sum_{n=1}^{3N_{\rm at}} |\mathbf{e}_i(\mathbf{q}n)|^2 \delta(\omega - \omega_{\mathbf{q}n}), \tag{4}$$

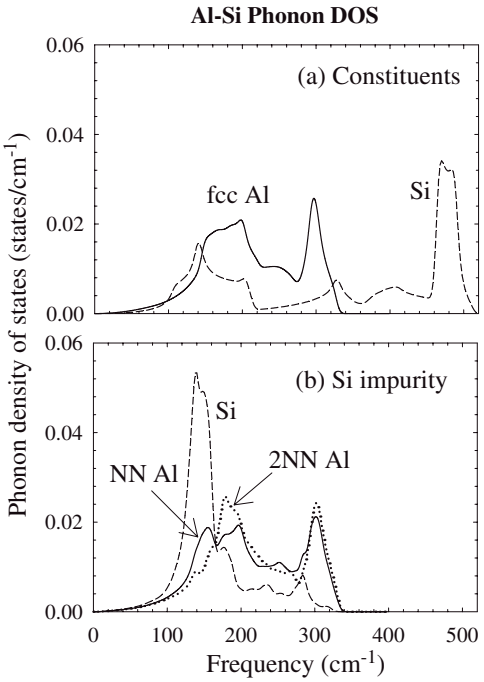

Figure 2. Calculated atom-projected phonon DOS around a Si impurity in Al (bottom panel), compared with the phonon DOS of fcc Al and diamond-structure Si (top panel). The lower panel shows LDA linear response results obtained using the 32-atom supercell.

where N_{at} is the number of atoms in the unit cell, MN_{at} is the total number of atoms in the crystal, $\omega_{\mathbf{q}n}$ is the frequency of a phonon mode with a wavevector $\mathbf{q}$ and branch index n, and $\mathbf{e}_i(\mathbf{q}n)$ is a normalized phonon eigenvector. Subscript i runs over all symmetry inequivalent atom types.

Figure 2(b) shows that the Si impurity-projected partial DOS is centred around much lower frequencies than the phonon DOS of diamond Si, which is represented by a dashed line in figure 2(a). Around the Si impurity, there is an additional slight softening of the partial phonon DOS for the nearest-neighbour (NN) shell of Al atoms. Noticeable changes are also observed in the second-nearest neighbour shell of Al atoms (see figure 2). Our findings are consistent with the experimental results of Chevrier *et al* [54, 55], who prepared supersaturated Al–Si solid solutions using high-pressure quench techniques. They found a significant phonon softening in the range of transverse-acoustic (TA) frequencies of Al and attributed this effect to a Si-induced decrease in the lattice shear modulus. A theoretical investigation of Si vibrations in fcc Al was performed by Caro *et al* [56] using an approximate first-principles scheme based on a minimal basis set and the Harris functional. Our results are broadly consistent with their conclusions, but there are important quantitative differences in the calculated phonon frequencies and lattice relaxations, which are probably caused by their use of an approximate scheme.

The total entropy of formation can be exactly partitioned into contributions $\Delta S_{\mathrm{vib}}(i)$ associated with individual atoms [11]. Indeed, above one-third of the characteristic Debye temperature (which is 428 K for Al and 645 K for Si [57]), the vibrational entropy is proportional to the logarithmic moment of the phonon DOS [29], $S_{\mathrm{vib}} \propto -\int \ln(\omega) g(\omega)\, \mathrm{d}\omega$.

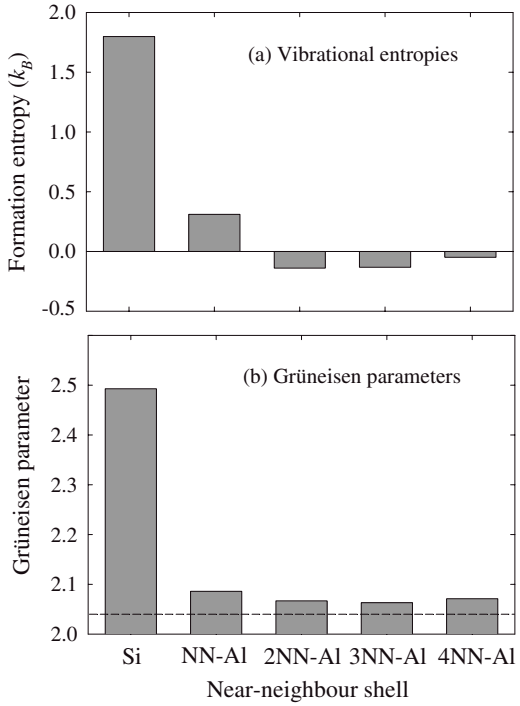

Figure 3. Atom-decomposed excess vibrational entropies $\Delta S_{\rm vib}(i)$ (top panel) and Grüneisen parameters $\gamma(i)$ (bottom panel). These results were obtained using the 32-atom supercell and LDA linear response method.

Using equation (4) to express the total $g(\omega)$ and subtracting the vibrational entropy of the pure constituents, gives the desired atomic decomposition. Application of this procedure to the partial DOS curves in figure 2 yields the values of $\Delta S_{\rm vib}(i)$ shown in figure 3(a). It is found that most of the total entropy of formation (1.8 $k_{\rm B}$ out of 2.2 $k_{\rm B}$) can be attributed to the Si impurity atom. There is an appreciable contribution to the formation entropy from the nearest-neighbour Al shell ($12 \times 0.026 = 0.31\ k_{\rm B}$); the effect of farther Al neighbours is insignificant. This suggests that most of the vibrational entropy contribution to the impurity $\Delta S_{\rm nc}$ is due to the relative softness of Al–Si bonds in comparison with Al–Al and Si–Si bonds in the pure constituents.

This conjecture is supported by the data in table 2, which gives the calculated nearest-neighbour bond lengths and longitudinal force constants in pure fcc Al, in diamond Si, and in the 32-atom Si impurity supercell. The longitudinal force constant $\Phi_l(ij)$ is defined as the largest negative eigenvalue of the 3×3 force constant matrix $\Phi_{\alpha\beta}(ij)$ between atoms i and j. For nearest neighbours, the largest eigenvalue always corresponds to an eigenvector connecting both sites, in accordance with the intuitive concept of longitudinal bond stiffness. As seen from table 2, the Al–Si force constant is found to be -0.92 eV Å^{-2}, softer than either the Al–Al force constant -1.36 eV Å^{-2} or the Si–Si force constant -7.93 eV Å^{-2}. As expected from intuitive properties of the covalent bonding in the diamond structure, the Si–Si bond exhibits the strongest longitudinal force constant. Another important property of interatomic forces, apparent from table 2, is a 13% increase in the Al–Al force constant between two Al atoms that share the Si impurity as one of their nearest neighbours. This increase occurs due to symmetry-imposed shortening of the Al–Al bond length in the vicinity of an impurity. Indeed,

Table 2. Comparison of bond lengths d (in Å), longitudinal force constants Φ_l (in eV Å^{-2}) and their rate of decrease upon lattice expansion, $\frac{a}{\Phi_l}\frac{\mathrm{d}\Phi_l}{\mathrm{d}a}$, in Al–Si alloys. Φ_l are defined as the largest (by absolute value) eigenvalue of the corresponding nearest-neighbour force constant matrix. All results are obtained using the LDA, NCPP and the linear response method.

Property	Pair	fcc Al	Diamond Si	Si impurity
	Al–Si			2.786
Bond length d	Al–Al	2.803		2.786[a]
	Si–Si		2.332	
NN force	Al–Si			−0.92
constant Φ_l	Al–Al	−1.36		−1.54[a]
	Si–Si		−7.93	
Grüneisen	Al–Si			−14.6
parameter $\frac{a}{\Phi_l}\frac{\mathrm{d}\Phi_l}{\mathrm{d}a}$	Al–Al	−10.6		−10.6[a]
	Si–Si		−9.4	

[a] These Al atoms share a nearest-neighbour Si impurity.

simple geometric considerations show that the bond length between two NN Al atoms around an impurity atom must be the same as the bond length between Al and the impurity atom (see table 2). Since d (Al–Si) is smaller than d (Al–Al) in FCC Al, the corresponding force constant is stiffer. Recently, a model that relates the bond stiffness to the bond length has been proposed [10, 15, 16]. It suggests that, for a given pair of atoms, the relationship between Φ_l and d is largely independent of the local environment and alloy composition. Our results for Al–Al force constants around the Si impurity are consistent with this idea.

We have shown that Si-induced lattice softening in the (Al) phase does not propagate much beyond the nearest-neighbour shell of Al atoms. It is interesting to note that a previous study of the Al–Sc system [11] found that a transition metal Sc impurity introduces a much more extensive elastic softening of the crystal lattice of fcc Al. The larger effect was attributed to a sizeable charge transfer to the Sc impurity and the surrounding complex of twelve NN Al atoms. Electronic Friedel oscillations and elastic effects due to size mismatch between Sc and Al were shown to combine, significantly softening Al–Al bonds up to the fourth-nearest neighbour shell. Neither charge transfer nor size mismatch are expected to be of comparable importance in the Al–Si system, which explains why force-constant perturbation is effectively contained within the nearest-neighbour shell.

3.3. Anharmonic effects and thermal expansion

Two important consequences of anharmonic lattice vibrations are thermal expansion and the associated phonon softening; both effects contribute to the free energies of alloy phases. Nevertheless, their influence upon the calculated alloy phase diagrams is generally thought to be small [9–11]. It is not immediately clear if this conclusion will hold for the Al–Si system, where thermal expansion properties of (Al) and (Si) solid-solution phases are very different. Indeed, consider the behaviour of phonon mode Grüneisen parameters, $\gamma_n(\mathbf{q}) = \frac{\mathrm{d}\ln\omega_n(\mathbf{q})}{\mathrm{d}\ln V}$, in pure Al and Si. In fcc Al (and other 'normal' solids), the Grüneisen parameter is positive, indicating that phonon frequencies, and thus the vibrational free energy, decrease with expanding volume. In contrast, Si has several transverse-acoustic phonon modes with negative Grüneisen parameters [52, 53]; it is one of the relatively few solids that is predicted to exhibit negative thermal expansion at low temperatures. Even though at high temperatures Si has a 'normal' positive coefficient of volume expansion, β, it is still an order of magnitude smaller than that of Al. A large disparity in the values of β for (Al) and (Si) phases indicates

that the quasiharmonic free energy difference may be strongly temperature-dependent, which in turn may influence the solvus boundary.

Phonon mode Grüneisen parameters have been evaluated for fcc Al, for diamond-structure Si, and for the 32-atom Si impurity cell using the linear response finite-difference method (see section 2). Effects of thermal expansion on the calculated phase diagram can be described using a thermodynamic Grüneisen parameter $\gamma_{\rm G}(T)$, representing a weighted average over all phonon modes:

$$\gamma_{\rm G}(T) = \frac{1}{MC_V(T)} \sum_{\mathbf{q}} \sum_{n=1}^{3N_{\rm at}} \gamma_{\mathbf{q}n} C\left(\frac{\hbar\omega_{\mathbf{q}n}}{k_{\rm B}T}\right), \tag{5}$$

where $C(x) = k_{\rm B}x^2/[4\sinh^2(x/2)]$ is the well-known phonon mode heat capacity function, and $C_V(T) = \frac{1}{M}\sum_{\mathbf{q}n} C\left(\frac{\hbar\omega_{\mathbf{q}n}}{k_{\rm B}T}\right)$ is the total fixed-volume heat capacity. At high temperatures, the heat capacity of phonons tends to a constant, $\lim_{x\to\infty} C(x) = k_{\rm B}$, and the thermodynamic Grüneisen parameter becomes a simple average over all phonon modes, $\gamma_{\rm G} = \frac{1}{MN_{\rm at}}\sum_{\mathbf{q}n}\gamma_{\mathbf{q}n}$. The calculated values of $\gamma_{\rm G}$ are given in table 1.

The rate of vibrational entropy increase due to thermal expansion at zero pressure is given by

$$\left(\frac{\partial S}{\partial T}\right)_{p=0} = \left(\frac{\partial S}{\partial V}\right)_T \left(\frac{\partial V}{\partial T}\right)_{p=0} = \beta\gamma_{\rm G}C_V = \frac{(C_V\gamma_{\rm G})^2}{V_0B_0}, \tag{6}$$

where V_0 and B_0 are the equilibrium $T = 0$ K volume and bulk modulus, respectively. In deriving equation (6), we have used a well-known expression for the coefficient of volume thermal expansion in cubic materials: $\beta = C_V\gamma_{\rm G}/(V_0B_0)$ [29]. Using the equilibrium lattice parameters, bulk moduli and Grüneisen coefficients from table 1, we obtain that at high temperatures the formation entropy $\Delta S_{\rm vib}$ increases at a rate of 0.88 $k_{\rm B}$ per 1000 K. This is a substantial effect, which at $T = 850$ K contributes more than 30% to the calculated vibrational entropy of formation. However, its effect on the free energy is partly compensated by a simultaneous increase in the internal energy ΔH. Indeed, assuming a linear volume expansion $V = V_0(1 + \beta T)$, we find that the internal energy will increase by $\delta E = \frac{B_0}{2V_0}(V - V_0)^2 = \frac{(C_V\gamma_{\rm G})^2}{2V_0B_0}T^2$. Adding the change in the entropy term given by equation (6), $-T\Delta S = -T^2\frac{\partial S}{\partial T}$, we find that the total free energy decrease due to thermal expansion is $\delta G_{\rm vib} = -\frac{(C_V\gamma_{\rm G}T)^2}{2V_0B_0}$, i.e. it is exactly one half of the change due to increase in the entropy. Using the derived $\delta G_{\rm vib}$ in equation (1), one finds that thermal expansion adds a multiplicative factor to the solubility $c_{\rm s}(T)$, which increases exponentially with temperature:

$$f_{\rm s}(T) = \exp\left[\frac{(C_V\gamma_{\rm G})^2}{2k_{\rm B}V_0B_0}T\right]. \tag{7}$$

The corresponding increase in the solubility of Si in Al is calculated to be 55% at $T = 850$ K. This is a relatively insignificant amount in comparison with the approximately ten-fold enhancement due to the harmonic vibrational entropy.

In the preceding discussion, we made two implicit physical assumptions. *Firstly*, we neglected the temperature dependence of β, C_V and $\gamma_{\rm G}$ in the derivation of equation (7); our numerical estimates used their high-temperature limiting values. Obviously, this assumption is not valid below the Debye temperature where quantum effects are important and β, C_V and $\gamma_{\rm G}$ are all T-dependent. However, this temperature region is usually quite narrow and can be neglected for our purposes. *Secondly*, equation (6) may become inaccurate near the melting point, where anharmonic finite phonon lifetime effects become important and the quasiharmonic approximation starts to break down. *Thirdly*, the simple regular-solution

formula (1) is valid only for compositions below 1–2 at.%. Thermal expansion contributions to ΔG increase linearly with temperature and thus become appreciable only at temperatures where the solubility is high enough that impurity–impurity interactions may invalidate the basic premise of the regular solution model.

It is conceptually useful to partition γ_{G} into contributions associated with individual atoms. This partitioning is done in a manner that is analogous to the definition of the partial phonon DOS in equation (4):

$$\gamma(i) = \frac{N_{\mathrm{at}}}{MC_V(T)} \sum_{\mathbf{q}} \sum_{n=1}^{3N_{\mathrm{at}}} |\mathbf{e}_i(\mathbf{q}n)|^2 \, \gamma_{\mathbf{q}n} \, C\left(\frac{\hbar\omega_{\mathbf{q}n}}{k_{\mathrm{B}}T}\right). \tag{8}$$

It is obvious that an average of $\gamma(i)$ over all atoms gives the thermodynamic Grüneisen parameter, $\gamma_{\mathrm{G}} = \frac{1}{N_{\mathrm{at}}} \sum_{i=1}^{N_{\mathrm{at}}} \gamma(i)$. Figure 3(b) shows the calculated partial Grüneisen parameters $\gamma(i)$ for a 32-atom Si impurity cell. It shows that the Si atom has a significantly above-average Grüneisen parameter $\gamma(\mathrm{Si}) = 2.5$. Furthermore, Al atoms in the nearest-neighbour shell also exhibit $\gamma(i)$ that is slightly higher than that of ideal fcc Al (the latter is shown as a dashed line in figure 3(b)). These properties indicate that not only is the Al–Si bond rather soft, but that it also softens more than Al–Al bonds upon increasing volume. This proposition is further supported by the data in table 2, showing the relative change in the nearest-neighbour force constants with the lattice parameter, $\frac{\mathrm{d}\ln\Phi_l}{\mathrm{d}\ln a}$. Indeed, the Al–Si longitudinal force constant softens upon increasing volume faster than either of the Al–Al or Si–Si force constants. Thus, Si impurities increase the thermal expansion of the (Al) phase. A similar conclusion was reached in a first-principles study of the vibrational entropy in Cu–Au [9], which found that thermal expansion was higher in phases with overall softer phonon frequencies, e.g. the disordered alloy had both a higher entropy and a larger Grüneisen parameter. In contrast, the Al–Sc system seems to exhibit the opposite effect since the thermal expansion was found to slightly *decrease* the solubility of Sc in Al [11].

3.4. GGA impurity free energies

To assess the importance of corrections to the LDA, we have used the generalized gradient approximation (GGA) of Perdew and Wang [31] to recalculate the excess enthalpy ΔH and entropy ΔS_{vib}. We found that the GGA removes most of the discrepancy between the calculated and measured solubilities by substantially increasing the formation energy of a Si impurity. The data in table 1 shows that the GGA predicts a formation enthalpy $\Delta H = +467$ meV per Si atom, which is close to the value of +504 meV per Si atom obtained from the analysis of experimental data of Dix and Heath [25] in section 3.1.

We have also recalculated the effect of the GGA on the vibrational entropy of a Si impurity. Since our linear response code is not programmed for the GGA, we have used VASP frozen phonon calculations to obtain all $\mathbf{q} = 0$ phonons in the 32- and 64-atom supercells. The calculated entropies of formation are $\Delta S_{\mathrm{vib}} = +2.4$ and $+2.6\,k_{\mathrm{B}}$ per Si atom using the 32- and 64-atom cells, respectively. These entropies are slightly higher than the corresponding LDA frozen-phonon values of +1.9 and $+2.3\,k_{\mathrm{B}}$ (see table 1). Increase in ΔS_{vib} is most likely caused by a slight lattice expansion of fcc Al when using the GGA. Indeed, in section 3.3 we showed that the Al–Si bond softens faster than either of the Al–Al or Si–Si bonds; therefore, the excess entropy of a Si impurity increases with the equilibrium volume of the (Al) phase. More quantitatively, we can use the thermal expansion data in table 1 to obtain an estimate of the magnitude of this effect. Using the relation $\left(\frac{\partial S}{\partial V}\right)_T \Delta V = \Delta V \gamma_{\mathrm{G}} C_V / V_0$, we get that, for the 32-atom cell, ΔS_{vib} should increase by $0.5\,k_{\mathrm{B}}$ if the equilibrium volume is expanded by

5%, corresponding to the GGA/LDA volume effect. This estimate is surprisingly (and perhaps a little fortuitously) consistent with the directly calculated change from +1.9 to +2.4 k_B.

Our findings for the change in ΔH and ΔS_{vib} are in line with the GGA results for Al and Si obtained by other authors. Firstly, it is well-known that gradient corrections tend to favour charge inhomogeneities and thus lower the energy of systems with inhomogeneous charge distribution [58]. This observation is confirmed by our calculated excess formation enthalpies, which are found to increase when going from the LDA to the GGA. Indeed, the charge distribution around a Si impurity in Al is much more homogeneous than the charge distribution in directionally bonded diamond Si, causing the GGA to favour the latter. Secondly, it is known that the LDA consistently predicts cohesive energies that are too high [59]. In contrast, the GGA generally provides cohesive energies that are much closer to the experimental values than those predicted by the LDA [60]. It is understood that this is also a consequence of the gradient corrections favouring the atom over the solid due to larger charge inhomogeneity in the latter. Furthermore, the GGA predicts lattice parameters that are almost always larger than the LDA values, and in many cases they are found to improve the agreement with the experiment [61–63]. For instance, the GGA lattice parameter of Al is found to be 4.045 Å, which is in excellent agreement with the experimental value of 4.05 Å. However, for diamond Si the GGA predicts an equilibrium lattice constant that is approximately 1% larger than the experimental value (5.48 versus 5.43 Å). These relatively small corrections to the equilibrium lattice parameters are expected to have negligible effects on the calculated formation energies, but their effect on vibrational properties is usually more important, since the phonon frequencies are quite sensitive to the equilibrium lattice parameter [64]. Thirdly, some studies have shown that the structural energy differences between different phases of Si are affected by the gradient corrections. In the case of the diamond $\rightarrow$ β-tin transition, the GGA was found to increase the transition pressure from 72 kbar (LDA) to 135 kbar [65], indicating that the gradient corrections favour the four-fold coordinated covalent diamond structure over the six-fold coordinated metallic β-tin structure. Again, this prediction of the GGA can be explained by a more inhomogeneous charge distribution in the diamond structure. It is also qualitatively consistent with our observation of increase in the formation energy of a Si impurity when going from the LDA to GGA.

Using the 64-atom GGA value of the vibrational entropy, $\Delta S_{vib} = +2.6\ k_B$/atom, we obtain that at $T = 850$ K the solubility is 2.3 at.%. The calculated solvus boundary is shown as a dash–dotted line in figure 1. As discussed in the previous section, thermal expansion is expected to increase this value by approximately 55%. A significant portion of the remaining discrepancy can be attributed to a remaining 7% error in the calculated enthalpy. Indeed, the value $\Delta S_{nc} = +2.7\ k_B$ per Si atom, extracted from the analysis of experimental data in section 3.1, is very close to the GGA value of ΔS_{vib}. However, corrections to the ideal-solution formula (1) could also alter the precise value of solubility. These corrections are not straightforward to evaluate as they require the knowledge of Si–Si interactions in the (Al) solid solution phase. The important conclusion is that the inclusion of vibrational entropy dramatically increases the calculated solubility and brings the GGA results in good agreement with experimental measurements.

4. Discussion and summary

Zener [66] was the first to suggest that vibrational entropy may have significant effects on the calculated alloy phase boundaries. He analysed the available solubility data for several Al-based alloys (including Al–Si) and, assuming that the enthalpy and entropy are independent of temperature, extracted ΔS_{nc} from an Arrhenius plot of $\ln c_s(T)$ versus $1/T$. Large values

of ΔS_{nc} were found in all cases. Our work confirms Zener's analysis and provides detailed physical insights into the microscopic causes for large vibrational entropy effects in Al–Si. We have demonstrated that vibrational contributions to the Gibbs free energy have a large effect on the solvus boundary in the Al–Si system. Using a wide variety of numerical methods and exchange–correlation functionals, in all cases the calculated vibrational entropy of formation of a Si impurity in fcc Al is found to be more than $+2\ k_B$ per Si atom, which leads to a roughly ten-fold increase in the solubility. This effect has been shown to originate from the much weaker bonding of Si atom in the solid solution (Al) phase than in the covalently bonded diamond Si structure. Thermal expansion effects are found to contribute a 55% increase in solubility at $T = 850$ K, which is relatively insignificant. Surprisingly, the widely used local-density approximation is shown to do a poor job of predicting the energy differences between the covalent and metallic bonding environments in the diamond-structure (Si) and fcc-based (Al) phases, respectively. The LDA underestimates the formation enthalpy of a Si impurity by approximately 0.2 eV, which leads to a very poor agreement between the calculated solvus and experimental data. This failure has been attributed to the neglect of charge inhomogeneity terms in the LDA exchange–correlation energy. The generalized gradient approximation of Perdew and Wang [31] does a much better job of describing the formation enthalpy, predicting a value of $\Delta H = +0.467$ eV, which is in good agreement with the value $\Delta H = +0.504$ eV extracted from the experimental solubility data. The success of the GGA is attributed to its tendency to favour charge inhomogeneities, decreasing the energy of the diamond (Si) phase relative to the solid-solution (Al) phase and thus increasing the impurity formation energy. Using the GGA, we obtain a solvus boundary that is in good agreement with the experimental data, while the LDA enthalpies are found to severely overestimate Si solubility in (Al).

Acknowledgments

VO gratefully acknowledges financial support from the National Science Foundation under programme DMR-0427638. Work at the Lawrence Livermore National Laboratory was performed under the auspices of the US Department of Energy, contract no. W-7405-Eng-48. Research at Northwestern was supported by the United States Department of Energy. Basic Energy Sciences Division under contract DE-FG02-01ER45910.

References

[1] Ducastelle F 1991 *Order and Phase Stability in Alloys* (New York: North-Holland)
[2] de Fontaine D 1994 *Solid State Phys.* **47** 33
[3] Zunger A 1994 First-principles statistical mechanics of semiconductor alloys and intermetallic compounds *Statics and Dynamics of Alloy Phase Transformations* (*NATO Advanced Study Institute, Series B: Physics* vol 319) ed P E A Turchi and A Gonis (New York: Plenum)
[4] Asta M, Ozoliņš V and Woodward C 2001 *JOM* **53** 16
[5] Ceder G, van der Ven A, Marianetti C and Morgan D 2000 *Model. Simul. Mater. Sci. Eng.* **8** 311
[6] Sanchez J M, Ducastelle F and Gratias D 1984 *Physica* A **128** 33
[7] Kattner U R 1997 *JOM* **49** 14
[8] van de Walle A, Ceder G and Waghmare U V 1998 *Phys. Rev. Lett.* **80** 4911
[9] Ozoliņš V, Wolverton C and Zunger A 1998 *Phys. Rev.* B **58** R5897
[10] van de Walle A and Ceder G 2000 *Phys. Rev.* B **61** 5972
[11] Ozoliņš V and Asta M 2001 *Phys. Rev. Lett.* **86** 448
[12] Asta M and Ozoliņš V 2001 *Phys. Rev.* B **64** 094104
[13] Wolverton C and Ozoliņš V 2001 *Phys. Rev. Lett.* **86** 5518
[14] Clouet E, Sanchez J M and Sigli C 2002 *Phys. Rev.* B **65** 094105
[15] van de Walle A and Ceder G 2002 *Rev. Mod. Phys.* **74** 11

[16] Wu E J, Ceder G and van de Walle A 2003 *Phys. Rev.* B **67** 134103
[17] Anthony L, Okamoto J K and Fultz B 1993 *Phys. Rev. Lett.* **70** 1128
[18] Anthony L, Nagel L J, Okamoto J K and Fultz B 1994 *Phys. Rev. Lett.* **73** 3034
[19] Fultz B, Anthony L, Nagel L J, Nicklow R M and Spooner S 1995 *Phys. Rev.* B **52** 3315
[20] Nagel L J, Anthony L and Fultz B 1995 *Phil. Mag. Lett.* **72** 421
[21] Fultz B, Stephens T A, Sturhahn W, Toellner T S and Alp E E 1998 *Phys. Rev. Lett.* **80** 3304
[22] Bogdanoff P D and Fultz B 1999 *Phil. Mag.* B **79** 753
[23] Bogdanoff P D, Fultz B and Rosenkranz S 1999 *Phys. Rev.* B **60** 3976
[24] Massalski T B (ed) 1990 *Binary Alloy Phase Diagrams* (Materials Park, OH: ASM International)
[25] Dix E H and Heath A C 1928 *Trans. AIME* **78** 164
[26] Phillips H W L J 1946 *J. Inst. Met.* **72** 158
[27] Phragmen G 1950 *J. Inst. Met.* **77** 498
[28] Fink W L and Van Horn K R 1931 *Trans. AIME* **93** 385
Fink W L and Van Horn K R 1931 *Trans. AIME* **93** 394
[29] Grimvall G 2002 *Thermophysical Properties of Matter* 2nd edn (Amsterdam: North-Holland)
[30] Dreizler R M and Gross E K U 1990 *Density Functional Theory: An Approach to the Quantum Many-Body Problem* (Berlin: Springer)
[31] Perdew J P and Wang Y 1992 *Phys. Rev.* B **45** 13244
[32] Perdew J P and Zunger A 1981 *Phys. Rev.* B **23** 5048
[33] Troullier N and Martins J L 1991 *Phys. Rev.* B **43** 1993
[34] Vanderbilt D 1990 *Phys. Rev.* B **41** 7892
[35] Kresse G and Hafner J 1993 *Phys. Rev.* B **47** 558
[36] Kresse G and Hafner J 1994 *J. Phys.: Condens. Matter* **6** 8245
[37] Kresse G and Furthmüller J 1996 *Comput. Mater. Sci.* **6** 15
[38] Kresse G and Furthmüller J 1996 *Phys. Rev.* B **54** 11169
[39] Louie S G, Froyen S and Cohen M L 1982 *Phys. Rev.* B **26** 1738
[40] Baroni S, Giannozzi P and Testa A 1987 *Phys. Rev. Lett.* **58** 1861
[41] Giannozzi P, de Gironcoli S, Pavone P and Baroni S 1991 *Phys. Rev.* B **43** 7231
[42] Ozoliņš V 1996 *PhD Thesis* Royal Institute of Technology, Stockholm, Sweden
[43] Froyen S 1989 *Phys. Rev.* B **39** 3168
[44] Chen Y, Fu C L, Ho K M and Harmon B N 1985 *Phys. Rev.* B **31** 6775
[45] Maradudin A A, Montroll E W and Weiss G H 1971 *Theory of Lattice Dynamics in the Harmonic Approximation* (New York: Academic)
[46] Touloukian Y S (ed) 1975 *Thermal Expansion: Metallic Elements and Alloys* (New York: Plenum)
[47] Touloukian Y S (ed) 1975 *Thermal Expansion—Nonmetallic Solids* (New York: Plenum)
[48] Chetty N, Weinert M, Rahman T S and Davenport J W 1995 *Phys. Rev.* B **52** 6313
[49] Turner D E, Zhu Z Z, Chan C T and Ho K M 1997 *Phys. Rev.* B **55** 13842
[50] Hatch J E 1984 *Aluminum: Properties and Physical Metallurgy* (Metals Park, OH: American Society for Metals)
[51] Hansen M and Anderko K 1958 *Constitution of Binary Alloys* 2nd edn (New York: McGraw-Hill)
[52] Pavone P and Baroni S 1994 *Solid State Commun.* **90** 295
[53] Rignanese G M, Michenaud J P and Gonze X 1996 *Phys. Rev.* B **53** 4488
[54] Chevrier J, Suck J B, Capponi J J and Perroux M 1988 *Phys. Rev. Lett.* **61** 554
[55] Chevrier J, Suck J B, Lasjaunias J C, Perroux M and Capponi J J 1994 *Phys. Rev.* B **49** 961
[56] Caro A, Drabold D A and Sankey O F 1994 *Phys. Rev.* B **49** 6647
[57] Kittel C 1996 *Introduction to Solid State Physics* 7th edn (New York: Wiley)
[58] Perdew J P, Chevary J A, Vosko S H, Jackson K A, Pederson M R, Singh D J and Fiolhais C 1992 *Phys. Rev.* B **46** 6671
[59] Moruzzi V L, Janak J F and Williams A R 1978 *Calculated Electronic Properties of Metals* (New York: Pergamon)
[60] Ziesche P, Kurth S and Perdew J P 1998 *Comput. Mater. Sci.* **11** 122
[61] Ozoliņš V and Körling M 1993 *Phys. Rev.* B **48** 18304
[62] Khein A, Singh D J and Umrigar C J 1995 *Phys. Rev.* B **51** 4105
[63] Delin A, Fast L, Johansson B, Eriksson O and Wills J M 1998 *Phys. Rev.* B **58** 4345
[64] Favot F and DalCorso A 1999 *Phys. Rev.* B **60** 11427
[65] DalCorso A, Pasquarello A, Baldereschi A and Car R 1996 *Phys. Rev.* B **53** 1180
[66] Zener C 1950 *Thermodynamics in Physical Metallurgy* ed C Zener (Cleveland, OH: ASM) p 16